Supplemental Document

optica

Cavity electro-optics in thin-film lithium niobate for efficient microwave-to-optical transduction: supplement

JEFFREY HOLZGRAFE,[1] NEIL SINCLAIR,[1,2] DI ZHU,[1,3] AMIRHASSAN SHAMS-ANSARI,[1] MARCO COLANGELO,[3] YAOWEN HU,[1,4] MIAN ZHANG,[1,5] KARL K. BERGGREN,[3] AND MARKO LONČAR[1,*]

[1] *John A. Paulson School of Engineering and Applied Sciences, Harvard University, 29 Oxford Street, Cambridge, Massachusetts 02138, USA*
[2] *Division of Physics, Mathematics and Astronomy, and Alliance for Quantum Technologies, California Institute of Technology, 1200 E. California Boulevard, Pasadena, California 91125, USA*
[3] *Research Laboratory of Electronics, Massachusetts Institute of Technology, 50 Vassar Street, Cambridge, Massachusetts 02139, USA*
[4] *Department of Physics, Harvard University, 17 Oxford Street, Cambridge, Massachusetts 02138, USA*
[5] *HyperLight Corporation, 501 Massachusetts Avenue, Cambridge, Massachusetts 02139, USA*
[*] *Corresponding author: loncar@seas.harvard.edu*

Supplement DOI: https://doi.org/10.6084/m9.figshare.13247216

Parent Article DOI: https://doi.org/10.1364/OPTICA.397513

Cavity electro-optics in thin-film lithium niobate for efficient microwave-to-optical transduction: supplementary material

JEFFREY HOLZGRAFE[1], NEIL SINCLAIR[1,2], DI ZHU[1,3], AMIRHASSAN SHAMS-ANSARI[1], MARCO COLANGELO[3], YAOWEN HU[1,4], MIAN ZHANG[1,5], KARL K. BERGGREN[3], AND MARKO LONČAR[1]

[1]John A. Paulson School of Engineering and Applied Sciences, Harvard University, 29 Oxford Street, Cambridge, Massachusetts 02138, USA
[2]Division of Physics, Mathematics and Astronomy, and Alliance for Quantum Technologies, California Institute of Technology, 1200 E. California Boulevard, Pasadena, California 91125, USA
[3]Research Laboratory of Electronics, Massachusetts Institute of Technology, 50 Vassar Street, Cambridge, Massachusetts 02139, USA
[4]Department of Physics, Harvard University, 17 Oxford Street, Cambridge, Massachusetts 02138, USA
[5]HyperLight Corporation, 501 Massachusetts Avenue, Cambridge, Massachusetts 02139, USA
[*]Corresponding author: loncar@seas.harvard.edu

Compiled September 20, 2020

This document provides supplementary information to "Cavity electro-optics in thin-film lithium niobate for efficient microwave-to-optical transduction," https://doi.org/10.1364/OPTICA.397513. It describes an analytical model of the transducer, simulations of piezoelectric loss, the measurement setup, measurements of the nonlinear broadening of the microwave resonator, and interventions that could lead to improved transducer performance.

1. THEORY OF CAVITY ELECTRO-OPTICS FOR MICROWAVE-TO-OPTICAL TRANSDUCTION

A. Optical modes

The optical modes used in our device are delocalized between two evanescently coupled ring resonators. These optical modes are governed by the Hamiltonian

$$H_{\text{opt}} = (\omega_o + \delta)a_1^\dagger a_1 + (\omega_o - \delta)a_2^\dagger a_2 + \mu\left(a_1^\dagger a_2 + a_1 a_2^\dagger\right), \quad \text{(S1)}$$

where a_1 and a_2 are respectively the annihilation operators for the bright and dark ring resonator modes, 2δ is the detuning between ring resonator modes, and μ is the evanescent coupling rate. This Hamiltonian can be diagonalized by the Bologliubov transformation

$$\begin{aligned} a_+ &= va_2 - ua_1, \\ a_- &= ua_2 + va_1. \end{aligned} \quad \text{(S2)}$$

Note that a_+ and a_- must obey a bosonic commutation relation $\left[a_i, a_j\right] = \delta_{ij}$, which requires that $u^2 + v^2 = 1$. For convenience, we set $u = \cos\frac{\theta}{2}$ and $v = \sin\frac{\theta}{2}$, where θ is a hybridization parameter. The Hamiltonian will be diagonalized for $\tan\theta = \frac{\mu}{\delta}$, giving

$$H_{\text{opt}} = \omega_+ a_+^\dagger a_+ + \omega_- a_-^\dagger a_-, \quad \text{(S3)}$$

where the resonance frequencies are $\omega_\pm = \omega_0 \pm \sqrt{\delta\omega^2 + \mu^2}$. These optical system eigenmodes at frequency $\omega_\pm$ will be used to calculate the interaction Hamiltonian.

The loss rates[1] of the photonic molecule modes change with the hybridization parameter θ. In the resolved sideband approximation ($2\mu \gg \kappa$, where κ is the typical optical mode loss rate), Eq. S2 also diagonalizes the open system, and the internal (i) and external (e) loss rates for the hybrid modes, $\kappa_{\pm,\{\text{i,e}\}}$, are given by

$$\begin{aligned} \kappa_{+,\{\text{i,e}\}} &= v^2\kappa_{2,\{\text{i,e}\}} + u^2\kappa_{1,\{\text{i,e}\}}, \\ \kappa_{-,\{\text{i,e}\}} &= u^2\kappa_{2,\{\text{i,e}\}} + v^2\kappa_{1,\{\text{i,e}\}}, \end{aligned} \quad \text{(S4)}$$

[1]Here, all loss rates κ refer to the energy decay rate. In other literature κ sometimes refers to the field amplitude decay rate, which is half the energy decay rate.

where $\kappa_{\{1,2\},\{i,e\}}$ are the intrinsic and extrinsic loss rates for the bright and dark ring resonator modes.

B. Triple-resonance transduction

Our electro-optic transducer has three resonant modes. The two optical photonic-molecule modes have electric fields $\vec{E}_{\pm}(\vec{r}) = \sqrt{\frac{\hbar\omega_{\pm}}{2\epsilon(\vec{r})V_{\pm}}}\left(\vec{\psi}_{\pm}(\vec{r})a_{\pm}e^{-i\omega_{\pm}t} + \text{h.c.}\right)$. The microwave mode has electric field $\vec{E}_m(\vec{r}) = \sqrt{\frac{\hbar\omega_m}{2Cd_{\text{eff}}^2}}\left(\vec{\psi}_m(\vec{r})be^{-i\omega_m t} + \text{h.c.}\right)$. Here $\omega_{\{\pm,m\}}$ are the resonance frequencies, ϵ is the dielectric permittivity, $V_{\pm}$ are effective mode volumes, $a_{\pm}$ and b are annihilation operators for the optical and microwave modes, $\vec{\psi}_{\{\pm,m\}}$ are the field profiles[2], C is the total capacitance of the microwave resonator, and d_{eff} is a constant with dimensions of length that relates the voltage on the microwave resonator's capacitor to the electric field at the center of the optical waveguide. For our device geometry, all three modes are polarized approximately along the Z-axis of the nonlinear crystal in the region of interest, so we can use a scalar interaction approximation. The three-wave mixing process used in our device can be described by a nonlinear energy density [1]

$$U = 2\epsilon_0\chi^{(2)}E_+E_-E_m, \tag{S5}$$

where ϵ_0 is the electric permittivity of free space and $\chi^{(2)}$ is the effective scalar second-order dielectric susceptibility.

The interaction Hamiltonian for this process can be obtained from Eq. S5 by inserting our expressions for the mode fields and considering only terms that vary slowly near the triple-resonance condition $\omega_m = \omega_+ - \omega_-$, which yields:

$$H_I = \hbar g_0\left(ba_-a_+^{\dagger} + b^{\dagger}a_-^{\dagger}a_+\right). \tag{S6}$$

The single-photon interaction strength is

$$g_0 = \frac{\chi^{(2)}\omega_{\text{opt}}}{d_{\text{eff}}V_{\text{opt}}n^2}\sqrt{\frac{\hbar\omega_m}{2C}}\int dV\psi_+^*\psi_-\psi_m, \tag{S7}$$

where n is the optical refractive index and the integral is taken over the nonlinear material. If a strong pump laser is tuned to the red optical mode, we can replace the a_- operator with its classical expectation value $a_- \to \langle a_-\rangle = \sqrt{n_-} = \sqrt{\frac{\kappa_{-,e}}{\Delta_-^2+(\kappa_-/2)^2}}\sqrt{\frac{P}{\hbar\omega_l}}$, where $\kappa_- = \kappa_{-,i} + \kappa_{-,e}$ is the total loss rates of the red optical mode, ω_l is the pump laser frequency, $\Delta_- = \omega_l - \omega_-$ is the pump detuning, and P is the pump power. Moving to a frame where the optical modes rotate at the pump laser frequency, the full Hamiltonian for our system is

$$H = -\Delta_+a_+^{\dagger}a_+ + \omega_m b^{\dagger}b + g\left(b^{\dagger}a_+ + ba_+^{\dagger}\right), \tag{S8}$$

where $\Delta_+ = \omega_l - \omega_+$ is the detuning of the pump from the blue optical mode, and $g = g_0\sqrt{n_-}$ is the pump-enhanced coupling rate.

We now use the above Hamiltonian to estimate the bidirectional transduction efficiency between continuous-wave (CW) optical and microwave signals. Consider two signal fields incident on the transducer: an optical signal a_{in} detuned from the pump by ω_p, and a microwave signal b_{in} with frequency $\omega_{b\text{in}}$. The semi-classical Heisenberg-Langevin equations of motion governing the interaction between the microwave and blue optical modes are

$$\begin{aligned}\frac{da_+}{dt} &= -\left(-i\Delta_+ + \frac{\kappa_+}{2}\right)a_+ - igb + \sqrt{\kappa_{+,e}}a_{\text{in}}e^{-i\omega_p t},\\ \frac{db}{dt} &= -\left(i\omega_m + \frac{\kappa_m}{2}\right)b - iga_+ + \sqrt{\kappa_{m,e}}b_{\text{in}}e^{-i\omega_{b\text{in}}t},\end{aligned} \tag{S9}$$

where κ_m and $\kappa_{m,e}$ are the total and external coupling rates for the microwave mode. The resonator modes couple to propagating output fields a_{out} and b_{out} via the input-output relations

$$a_{\text{out}} = a_{\text{in}} - \sqrt{\kappa_{+,e}}a_+, \qquad b_{\text{out}} = b_{\text{in}} - \sqrt{\kappa_{b,e}}b. \tag{S10}$$

In the steady state, Eqs. S9 and S10 yield the frequency-domain transduction scattering matrix

$$\begin{bmatrix}a_{\text{out}}\\ b_{\text{out}}\end{bmatrix} = \begin{bmatrix}S_{\text{oo}} & S_{\text{oe}}\\ S_{\text{eo}} & S_{\text{ee}}\end{bmatrix}\begin{bmatrix}a_{\text{in}}\\ b_{\text{in}}\end{bmatrix}, \tag{S11}$$

where

$$\begin{aligned}S_{\text{oo}} &= 1 - \frac{\kappa_{+,e}}{-i\left(\Delta_+ + \omega_p\right) + \frac{\kappa_+}{2} + \frac{g^2}{i(\omega_m-\omega_p)+\kappa_m/2}},\\ S_{\text{oe}} &= \frac{ig\sqrt{\kappa_{+,e}\kappa_{b,e}}}{\left[i\left(\omega_m - \omega_{b\text{in}}\right) + \frac{\kappa_m}{2}\right]\left[-i\left(\Delta_+ + \omega_{b\text{in}}\right) + \frac{\kappa_+}{2}\right] + g^2},\\ S_{\text{eo}} &= \frac{ig\sqrt{\kappa_{+,e}\kappa_{b,e}}}{\left[i\left(\omega_m - \omega_p\right) + \frac{\kappa_m}{2}\right]\left[-i\left(\Delta_+ + \omega_p\right) + \frac{\kappa_+}{2}\right] + g^2},\\ S_{\text{ee}} &= 1 - \frac{\kappa_{m,e}}{i\left(\omega_m - \omega_{b\text{in}}\right) + \frac{\kappa_m}{2} + \frac{g^2}{-i(\Delta_+ + \omega_{b\text{in}})+\kappa_+/2}}.\end{aligned}$$

The conversion is symmetric, and the on-chip transduction efficiency can be written as

$$\begin{aligned}\eta_{\{\text{oe,eo}\}}(\omega) &= |S_{\{\text{oe,eo}\}}|^2\\ &= \frac{\kappa_{m,e}\kappa_{+,e}}{\kappa_m\kappa_+}\frac{4C}{\left|C + \left[\frac{-2i(\Delta_+ + \omega)}{\kappa_+} + 1\right]\left[\frac{2i(\omega_m - \omega)}{\kappa_m} + 1\right]\right|^2},\end{aligned} \tag{S12}$$

where ω is the excitation frequency, and $C = \frac{4g^2n_-}{\kappa_+\kappa_m}$ is the electro-optic cooperativity. At the triple-resonance condition, where $\omega = -\Delta_+ = \omega_m$, this efficiency takes the form

$$\eta_{\{\text{oe,eo}\}}(\omega) = \underbrace{\frac{\kappa_{m,e}\kappa_{+,e}}{\kappa_m\kappa_+}}_{\text{extraction efficiency}} \times \underbrace{\frac{4C}{(1+C)^2}}_{\text{internal efficiency}}. \tag{S13}$$

The first term represents the efficiency associated with getting a photon into and out of the converter, while the second term gives the transduction efficiency inside the converter.

C. Double-resonance transduction

When the converter is operated far-detuned from the triple-resonance condition, a double-resonance transduction process can become a significant contribution to the total transduction efficiency. In this process, optical photons in the red optical mode can be scattered between the pump frequency and a blue-shifted sideband. This sideband field is far-detuned from the red optical mode relative the mode's linewidth in our experiments, so the transduction efficiency for this process is low, but it can

[2] We assume a lumped-element model for the microwave mode and normalized it so $|\psi_m|^2 = 1$ at the center of the optical mode cross section in areas covered by the capacitor.

be larger than that of the triple-resonance process when the splitting between red and blue optical modes is much larger than the microwave frequency. This double-resonance process is the origin of the bias-voltage independent response for large negative voltages in Figs. 3(b) and 3(c) of the main text. The nonlinear energy density that describes this double-resonance process is [1]

$$U = \epsilon_0 \chi^{(2)} E_m E_-^2 \tag{S14}$$

which produces the Hamiltonian

$$H_I = \hbar g_{0,\mathrm{dr}} \left(b a_-^\dagger a_- + b^\dagger a_-^\dagger a_- \right), \tag{S15}$$

where

$$g_{0,\mathrm{dr}} = \frac{\chi^{(2)} \omega_{\mathrm{opt}}}{d_{\mathrm{eff}} V_{\mathrm{opt}} n^2} \sqrt{\frac{\hbar \omega_m}{2C}} \int dV |\psi_+|^2 \psi_m. \tag{S16}$$

Following the usual linearization procedure for the strongly pumped a_- mode [2], we approximate $a_- \approx \langle a_- \rangle + \delta a_-$, where δa_- is a small fluctuating perturbation to the field in the red optical mode. Keeping terms of order $\langle a_- \rangle$, the linearized interaction Hamiltonian is

$$H_I = \hbar g_{\mathrm{dr}} \left(\delta a_-^\dagger + \delta a_- \right) \left(b^\dagger + b \right), \tag{S17}$$

where $g_{\mathrm{dr}} = g_{0,\mathrm{dr}} \langle a_- \rangle$. This Hamiltonian contains both the desired beam-splitter terms and parametric amplification terms which cause optical down conversion, and since the pump is nearly resonant with the red optical mode, both types of terms are significant. In a frame where the optical mode rotates along with the laser, the semi-classical Heisenberg-Langevin equations of motion for double-resonance microwave-to-optical transduction are

$$\begin{aligned} \frac{d\left(\delta a_-\right)}{dt} &= -\left(-i\Delta_- + \frac{\kappa_-}{2}\right) \delta a_- - i g_{\mathrm{dr}} \left(b + b^\dagger \right), \\ \frac{db}{dt} &= -\left(i\omega_m + \frac{\kappa_m}{2} \right) b - i g_{\mathrm{dr}} \left(\delta a_- + \delta a_-^\dagger \right) + \sqrt{\kappa_{m,e}} b_{\mathrm{in}} e^{-i\omega t}. \end{aligned} \tag{S18}$$

For simplicity, we assume that the double resonance process operates in the weak coupling regime, so that back-action of the optical fields on the microwave field can be neglected[3]. We take the ansatz solution

$$\begin{aligned} \delta a_-(t) &= A_+ e^{-i\omega t} + A_- e^{i\omega t}, \\ b(t) &= B e^{-i\omega t}, \end{aligned} \tag{S19}$$

and find

$$\begin{aligned} B &= \frac{\sqrt{\kappa_{m,e}} b_{\mathrm{in}}}{i\left(\omega_m - \omega\right) + \kappa_m/2} \\ A_\pm &= \frac{-i g_{\mathrm{dr}} B}{-i\left(\Delta_- \pm \omega\right) + \kappa_-/2}. \end{aligned} \tag{S20}$$

The transmitted optical sideband field due to double-resonance transduction is $\delta a_{\mathrm{out}} = -\sqrt{\kappa_{-,e}} \delta a_-$, and hence the total apparent transduction efficiency[4], including both double- and triple-resonance transduction, is

$$\eta_{\mathrm{oe}} = |S_{\mathrm{eo}} - \sqrt{\kappa_{-,e}} A_+ - \sqrt{\kappa_{-,e}} A_-^*|^2. \tag{S21}$$

D. Estimating the electro-optic interaction strength

The triple-resonance interaction strength g_0 (Eq. S7) can be cast in a form more useful for designing the transducer. Assuming that the electric field created by the capacitor is oriented along the lithium niobate's Z crystal axis and uniform across the optical mode (a good approximation for our device geometry), and that the microwave resonator drives the optical resonators with opposite phase and behaves as a lumped-element system, we find

$$g_0(\theta) = \frac{r_{33} n_e^2 \hbar \omega_o \Gamma \alpha \sin(\theta)}{4 d_{\mathrm{eff}}} \sqrt{\frac{\hbar \omega_m}{2C}}, \tag{S22}$$

here $r_{33} = 2\chi^{(2)}/n^4$ is the relevant electro-optic coefficient, n_e is the extraordinary refractive index of lithium niobate, Γ is an optical mode confinement factor, α is an electrode coverage parameter with a maximum value of 2 for full coverage of both optical resonators, and θ is the optical mode mixing parameter described above[5]. From this equation, it is clear that the interaction strength can be maximized by creating a microwave resonator with closely spaced electrodes, low total capacitance, and full coverage of the optical resonators.

The calculated values for key device parameters are given in Table S1. Using these results, we estimate $g_0(\theta = \pi) = 2\pi \times 1.0$ kHz.

Table S1. Transducer device parameters for calculating the electro-optic interaction strength

Parameter	Value	Estimation method
Γ	0.93	Optical mode simulation
α	0.72	Calculated from device geometry
d_{eff}	15 µm	EO cross section simulation
C	120 fF	Full-wave simulation as in [3]

2. MICROWAVE RESONATOR AND PIEZOELECTRIC LOSS

To minimize the microwave mode volume and maximize the single-photon interaction strength, we designed a superconducting quasi-lumped microwave LC resonator, which is (predominantly) capacitvely coupled to a 50 Ω characteristic impedance coplanar waveguide. The niobium nitride superconducting film used to make the resonator has a relatively high sheet kinetic inductance of ~ 5 pH/□, which allows for a more compact inductor design. Using a method of moments simulation [4], we estimate the effective lumped capacitance and inductance by varying the magnitude of a small ideal capacitance added in parallel. The change in resonance frequency with added capacitance allows us to determine the total capacitance and inductance [3]. We simulate the lumped element circuit parameters to be $C = 120$ fF, $L = 6.7$ nH, and $\omega_m/2\pi = (LC)^{-1/2} = 5.6$ GHz. We attribute the somewhat lower measured resonance frequency

[3] i.e. the term $-i g_{\mathrm{dr}} \left(\delta a_- + \delta a_-^\dagger \right)$ can be dropped

[4] The existence of multiple optical sidebands in regimes where double-resonance transduction is significant means that transduction efficiency must be carefully defined. In our experiments, we measure only the transmission of a microwave signal from the transducer's input to the photoreceiver's output, and we cannot differentiate multiple optical sidebands. As such, we define transduction efficiency for multiple sidebands as the apparent transduction efficiency: i.e. the equivalent single-sideband transduction efficiency which would produce the observed signal. Note that this distinction between apparent and true transduction efficiency is significant only in far-detuned regimes of bias voltage sweeps, not near the triple-resonance condition where maximum transduction efficiency occurs.

[5] Note that the values of g_0 used in the main text are quoted for the optical mode splitting (and hence the value of the hybridization parameter θ) which maximizes transduction efficiency. The maximum transduction efficiency is obtained for $\theta \approx 0.7\pi$ in our device.

to variations in the as-fabricated geometry of the devices. In particular, the width of the meander inductor is narrower than designed due to a small degree of mask erosion.

We use a two-dimensional finite element model to simulate the piezoelectric loss of the microwave resonator. In this frequency-domain simulation, a voltage is applied to the capacitor electrodes at frequency ω, and the time-averaged electrostatic energy $E_{\text{electrostatic}}$ and acoustic power absorbed by the perfectly-matched layer P_{acoustic} are calculated. The quality factor set by piezoelectric-loss is then given by

$$Q = \frac{\omega E_{\text{electrostatic}}}{P_{\text{acoustic}}}. \tag{S23}$$

The two-dimensional nature of the simulation means that acoustic modes with out-of-plane (i.e. along the waveguide) propagation or strain are neglected. Modes with an out-of-plane propagation direction couple weakly to the microwave resonator because the capacitor is much longer than the acoustic wavelength at the relevant ~GHz frequencies. Modes with out-of-plane stress also couple weakly to the microwave resonator for X-cut lithium niobate because of lithium niobate's piezoelectric coefficients. For example, when applying the electric field along the Z crystal axis in our device the d_{33} piezoelectric coefficient, which creates in-plane stress, dominates over other components.

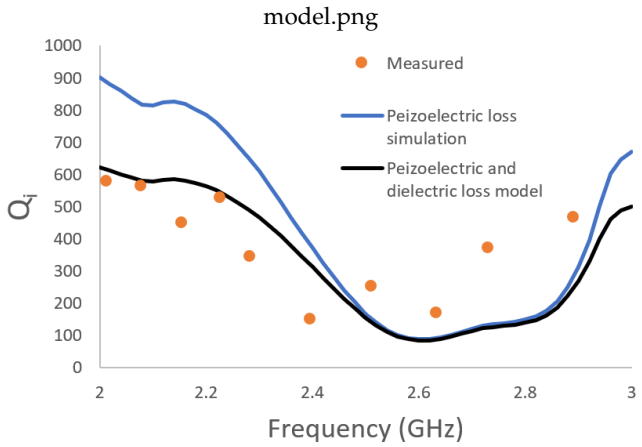

Fig. S1. Microwave loss for varied resonance frequency. Measured data was inferred from transmission spectra ($T = 1$ K) of LC resonators similar to those described in the main text. The piezoelectric loss model is based on the two-dimensional simulations described above. The dielectric loss model adds an additional wideband loss corresponding to $Q_{\text{clad}} = 2000$

To verify the role of piezoelectric loss in our device, we fabricated an array of transducer devices without etched optical waveguides — i.e. just the microwave resonators on the material stack described in the main text. We created devices with microwave resonance frequencies varying from 2 to 3 GHz by varying the inductor size. Measuring transmission spectra at $T = 1$ K, we extract the intrinsic loss for the resonators, shown in Fig. S1. The sharp and non-monotonic frequency dependence of the microwave loss is evidence for piezoelectric loss, as most other loss mechanisms vary slowly with frequency in this range. Our simulation results qualitatively match the sharp frequency dependence in the measured data, but predict much higher maximum intrinsic quality factors. We attribute this discrepancy to additional wideband dielectric loss in the amorphous cladding material. To confirm this, we fabricated devices without lithium niobate or amorphous oxide layers on a high-resistivity silicon substrate and found intrinsic quality factors exceeding 10^4.

3. MEASUREMENT SETUP AND TRANSDUCTION EFFICIENCY CALIBRATION

Details of the measurement setup are shown in Figure S2. To calibrate the transduction efficiency, we perform the following procedure before every set of measurements.

First, with the laser frequency detuned far from the optical resonance, we measure the optical power into and out of the device under test (DUT). After correcting for measured asymmetric losses in the optical fibers going into the cryostat, we assume the loss at both input and output grating couplers to be symmetric. Based on measurements of a large number of grating couplers, we estimate the coupler-to-coupler variation in insertion loss to be less than 0.4 dB. Next, we measure the optical power arriving at the output of the analysis arm using the DC power meter. These measurements allow us to estimate the optical insertion loss from the DUT to the end of the analysis arm $\eta_{\text{optical}} = \eta_{\text{coupler}} \cdot \eta_{\text{fiber}}$, as well as the on-chip optical power.

Next, we calibrate the response of the 10 GHz-bandwidth photoreceiver by using port V1 to generate a single optical sideband. We measure the signal in the analysis arm using the high-resolution optical spectrum analyzer (which allows us to directly measure the relative power of the sideband and carrier $P_{\text{sideband}}/P_{\text{pump}}$), the calibrated DC power meter (which measures the total power $P_{\text{sideband}} + P_{\text{pump}}$), and the 10 GHz photoreceiver. These measurements allow us to estimate the detector response parameter $A_{\text{det.}}$, defined so that $P_{\text{det.}} = A_{\text{det.}} P_{\text{sideband}} P_{\text{pump}}$.

During the transduction measurement, when the laser frequency is locked to an optical mode, measurements of the total optical power and the 10 GHz photoreceiver response allow us to infer the power in the upconverted optical sideband P_{sideband}, based on the above photoreceiver calibration. The gain provided by the erbium-doped fiber amplifier (EDFA), if in use, can be estimated by measuring the photoreceiver response with and without the EDFA in the optical path. Finally, the calibrated transduction efficiency is given by

$$\eta = \frac{\omega_m P_{\text{sideband}}}{\omega_o P_{\text{in}} \eta_{\text{optical}} \eta_{\text{cable}}}, \tag{S24}$$

where P_{in} is the input microwave power at port V1A and η_{cable} is the measured insertion loss from port V1A to the DUT.

4. MICROWAVE RESONATOR NONLINEARITY

The superconducting NbN film is deposited using DC magnetron sputtering at room temperature with an RF bias on the substrate holder. The film has a thickness of ~44 nm, room-temperature sheet resistance of 52 Ω/square, and a transition temperature T_c of ~10 K. At high microwave powers, the superconducting resonator undergoes nonlinear oscillations [5], as shown in Fig. S3. In the actual experiment, the drive power is kept below -30 dBm, and the nonlinear dynamics are therefore small.

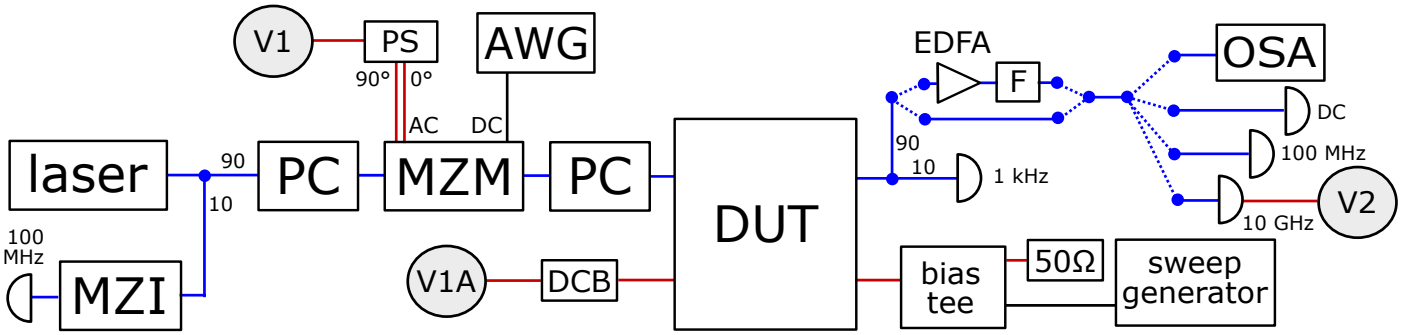

Fig. S2. Simplified diagram of the transduction measurement setup. Laser emission passes through polarization controllers (PC) and is modulated by a Mach-Zehnder modulator (MZM). A fraction of the emission is sent to a 100 MHz-bandwidth detector after passing through a Mach-Zehnder interferometer (MZI) of ∼1 m path length difference to precisely track sweeps of laser wavelength. The MZM is arranged for either GHz-frequency optical single-sideband modulation using a phase-shifted (PS) dual drive through a high-frequency port, or low-frequency amplitude modulation through a bias port, controlled by an arbitrary waveform generator (AWG). Focusing grating couplers (≈10 dB insertion loss) couple light from optical fibers into the device under test (DUT), which is cooled to $T \approx 1$ K inside a closed-cycle cryostat. The light collected from the DUT is split into an analysis arm (90%) and a 1 kHz photoreceiver (10%), whose signal is used to lock the laser frequency to an optical mode. The analysis arm passes through several optical switches (dotted blue lines) which allow for optional and repeatable insertion of an erbium-doped fiber amplifier (EDFA) and optical filter (F, 0.2nm bandwidth). The analysis arm can be sent to an optical spectrum analyzer (OSA) for sideband calibration, a DC optical power meter for power calibration, a 100 MHz photoreceiver for measuring transmission spectra, or a 10 GHz photoreceiver for detecting transduction. The bias voltage of the DUT is controlled by a sweep generator through a bias tee. A vector network analyzer (VNA) can be connected to microwave port V1A, which is protected by a DC block (DCB) capacitor, to excite the DUT. The upconverted optical signal can be detected at port V2. In an alternative measurement setup, the transmission of an optical sideband can be monitored by connecting the VNA to the optical single-sideband modulator (port V1).

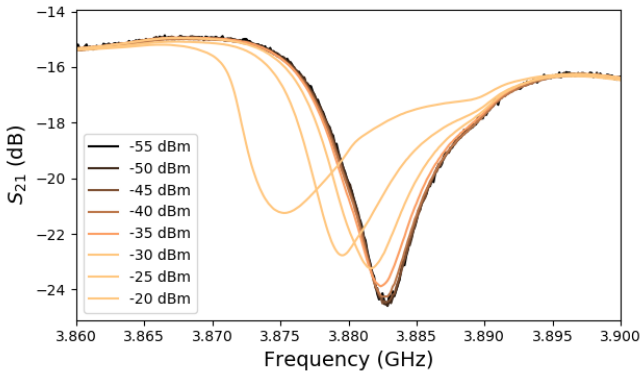

Fig. S3. Effect of microwave power on transmission spectrum. Microwave input powers above about −40 dBm at port V1A (∼ −48 dBm on-chip) produce distorted transmission spectra due to nonlinear dynamics. [5]

5. INTERVENTIONS FOR IMPROVED TRANSDUCER PERFORMANCE

Besides the improvements described in the conclusion of the main text, there are several other changes that can be made to enhance device performance: First, the electrode coverage fraction of the microwave resonator can be improved by at least 2-fold, for example by using a higher aspect ratio racetrack resonator, extending coverage to curved sections of the waveguides, and integrating the bias capacitor with the resonator. Second, using single-sided microwave coupling (as opposed to the two-sided coupling used here, where the cavity field is coupled to both right and left propagating modes) would eliminate an effective loss channel. Third, the capacitance of the microwave resonator can be reduced, increasing the single-photon electro-optic coupling rate. Straightforward ways to do this might include using higher-impedance spiral inductors or nesting the two optical resonators to reduce overall device size and parasitic capacitance. Photonic crystal modulators [6] would enable significantly smaller device footprint and microwave capacitance (in conjunction with high-impedance inductors), but may involve trade-offs in terms of optical loss and photoconductive effects. Finally, the optical pump can be tuned on-resonance with the optical mode, increasing the pump-enhanced coupling rate.

REFERENCES

1. J. A. Armstrong, N. Bloembergen, J. Ducuing, and P. S. Pershan, "Interactions between Light Waves in a Nonlinear Dielectric," Phys. Rev. **127**, 1918–1939 (1962).
2. M. Aspelmeyer, T. J. Kippenberg, and F. Marquardt, "Cavity optomechanics," Rev. Mod. Phys. **86**, 1391–1452 (2014).
3. J. M. Fink, M. Kalaee, A. Pitanti, R. Norte, L. Heinzle, M. Davanço, K. Srinivasan, and O. Painter, "Quantum electrome-

chanics on silicon nitride nanomembranes," Nat. Commun. **7**, 12396 (2016).
4. "Sonnet Software Inc." http://www.sonnetsoftware.com/.
5. B. Abdo, E. Segev, O. Shtempluck, and E. Buks, "Nonlinear dynamics in the resonance line shape of NbN superconducting resonators," Phys. Rev. B **73**, 134513 (2006).
6. M. Li, J. Ling, Y. He, U. A. Javid, S. Xue, and Q. Lin, "Lithium niobate photonic-crystal electro-optic modulator," Nat. Commun. **11**, 4123 (2020).